Detection of wheat powdery mildew based on hyperspectral reflectance through SPA and PLS-LDA

Imran Haider Khan[1,2], Haiyan Liu[1,2], Tao Cheng[1,2], Yongchao Tian[1,2], Qiang Cao[1,2], Yan Zhu[1,2], Weixing Cao[1,2], Xia Yao[1,2*]

(1. College of Agronomy, *Nanjing Agricultural University, Nanjing, Jiangsu 210095, China*;
2. *Jiangsu Key Laboratory for Information Agriculture, Nanjing, Jiangsu 210095, China*)

Abstract: The accurate recognition and quantitative assessment at the early stage of wheat powdery mildew (*Blumeria graminis* f. sp. *tritici*) are vital for precision crop management for spraying the fungicides, reducing the cost, protecting the environment and enhancing the quality of crop. However, early disease detection remained highly difficult due to the subtle changes in the physiology and phenology of the plants at early infection stage. In this study, two wheat cultivars with different disease resistances were inoculated by the powdery mildew, hyperspectral reflectance and physiological parameters of leaves were obtained after inoculation at early stem elongation stage. The major contribution of this study is to extract sensitive wavebands and vegetation indices using sub-window permutation analysis (SPA) by fully exploiting the hyperspectral data for early disease identification. Extracted sensitive features by SPA were then used as input in partial least squares-linear discriminant analysis (PLS-LDA) recognition model to classify the healthy and diseased wheat leaves. Finally, validation was carried out with independent data to verify the accuracy of the recognition model. The results indicated that (1) the pigment contents and photosynthetic capacity were changed slightly at the early infection stage but decreased rapidly with the aggravation of the disease severity; (2) the visible and the near infrared bands were the most sensitive to the disease at early infection stage; (3) the overall accuracy of the PLS-LDA model constructed with the sensitive features extracted by SPA method performed better than features selected conventionally by correlation analysis. The calibration and validation accuracies at 5% disease severity were 85.12 and 84.43% for model based on wavelength features and were 82.14 and 85.63 for model constructed with spectral indices features extracted by SPA, respectively. In conclusion, SPA is a new effective strategy for feature selection which has not been yet used in plant disease research, having the benefit of considering cooperative effect among different variables and demonstrated the potential of early disease detection. Such a technique can be an efficient and economical substitute to conventional methods, especially in case of high throughput hyperspectral crop sensing.

Keywords: wheat powdery mildew, early detection, hyperspectral reflectance, fungicide spraying, sub-window permutation analysis (SPA), PLS-LDA
DOI: 10.33440/j.ijpaa.20200301.67

Citation: Khan I H, Liu H Y, Cheng T, Tian Y C, Cao Q, Zhu Y, Cao W X, Yao X. Detection of wheat powdery mildew based on hyperspectral reflectance through SPA and PLS-LDA. Int J Precis Agric Aviat, 2020; 3(1): 13–22.

1 Introduction

Wheat is one of the most widely grown food crops in the world. Powdery mildew (*Blumeria graminis* f. sp. *tritici*), as a serious fungal disease, has become one of the most damaging and the most common diseases in wheat production with the highest incidence and the most harmful damage. In recent years, 5.9 million to 7 million hectares of wheat fields have been suffered from the incidence of powdery mildew in China, and millions of tons of wheat yield were reduced during a serious breakout of the powdery mildew disease[1]. Therefore, early detection of powdery mildew and quantitative monitoring of the disease severity are the key to precision crop managements for precise application of fungicides, ecological safety, and yield loss reduction. However, traditional field survey is time-consuming and erroneous depending on the knowledge and experience of the investigator. Remote sensing can be used as an alternative to real-time monitoring of crop health, especially hyperspectral technology that has been demonstrated in the early detection of diseases[2-4].

To recognize and classify crop diseases based on hyperspectral data, identification of sensitive bands or spectral features sensitive to the disease is of great significance. Lorenzen et al.[5] revealed that spectral reflectance of the leaves in the visible spectral region from 422 nm to 712 nm increased significantly after 6 days of inoculation, and a significant decrease in the near-infrared range was observed after 10 days of inoculation. Graeff et al.[6] found

Received date: 2019-12-30 **Accepted date:** 2020-03-16
Biographies: Imran Haider Khan, Doctoral student, research interests: agriculture remote sensing, growth monitoring and crop physiology, Email: imranhaiderkhan110@hotmail.com; **Haiyan Liu,** master student, research interests: disease detection with deep learning, Email: 2018101173@njau.edu.cn; **Tao Cheng,** PhD, research interests: crop growth monitoring , Email: tcheng@njau.edu.cn; **Qiang Cao,** PhD, research interests: crop growth monitoring and diagnosis, E-mail: qiangcao@njau.edu.cn; **Yongchao Tian,** PhD, research interests: crop growth monitoring and diagnosis, Email: yctian@njau.edu.cn; **Yan Zhu,** PhD, Professor, research interests: crop growth model, Email: yanzhu@njau.edu.cn**; Weixing Cao,** PhD, Professor, research interests: smart agriculture, Email: caow@njau.edu.cn
***Corresponding author: Xia Yao,** PhD, research interests: crop growth, stress and biochemical parameters based on hyperspectral / sunlight-induced chlorophyll fluorescence / LiDAR / UAV. Email: yaoxia@njau.edu.cn.

that the reflectance within the range of 490-780 nm was sensitive to leaf damage caused by wheat powdery mildew infections. In addition to reflectance, the derivative spectral features[7-9], spectral vegetation indices[10,11] and spectral disease indices[12-14] have shown the potential to diagnose plant diseases. For example, Zhang et al.[15] examined 32 spectral indices using t-test and correlation analysis and applied partial least square regression (PLSR) and multivariate linear regression (MLR) for estimating wheat powdery mildew at medium and late stage of disease. Cao et al.[16] suggested that the red-edge peak of hyperspectral canopy reflectance was the most sensitive parameter for powdery mildew detection. However, those studies focused on the limited spectrometry of certain wavelengths/bands and selected the sensitive wavebands based on empirical methods. As a result, some characteristic bands that reflect crop diseases have not been exploited and utilized. Moreover, the stability and generalization of features extracted by empirical methods are debatable. Most of them emphasized middle and late stage of disease and a few focused on early infection stage.

To address the limitations, machine learning has been employed to classify and identify crop diseases, such as support vector machine (SVM)[4], soft independent modeling of classification analogies (SIMCA), pattern recognition method[17], principal component spectra and probabilistic neural network[18,19] and wavelet analysis (WA)[20,21]. For example, Hamed Hamid Muhammed[22,23] used the feature-vector-based analysis (FVBA) method to determine the feature waveband of the disease sensitivity from the hyper spectrum of 360-900 nm. Moshou[24] used neural network (NN) to distinguish the disease which improved the accuracy of monitoring the disease status. Further, Moshou[25] recognized the crop diseases based on self-organization map with more accurate performance, which was integration of hyperspectral information with fluorescent imaging show. In addition to disease detection, some researchers also developed the distribution map of the crop diseases at the field and regional level[26].

It can be learnt that various machine learning methods such as Support Vector Machines (SVMs), k nearest neighbors, K-means, Decision Trees, CWT and artificial neural networks (ANNs) have been employed in agricultural research for detection of different disease of various plants based on different spectral features but the knowledge about detection of wheat powdery mildew at early stage by machine learning method is still limited. Our focus is automatic detection of wheat powdery mildew at early stage based on hyperspectral data by a new SPA method which has not been yet used in agricultural research.

In view of the fact that plant diseases are frequently associated with particular visual and physiological changes of their host plants, we employed a comprehensive methodology based on the combination of different wavebands and VIs acquired from hyperspectral data and applied SPA to completely exploit their combined information, with a special focus on early detection. Along with spectral analyses, we also monitored dynamic variations of physiological and biochemical parameters of wheat in response to powdery mildew stress. The early stage, in this paper, is defined as the period before the heading stage with 5% of leaf disease severity. Given that only subtle changes occurred in the internal structure and external symptoms of the plants, advanced methods are crucial to enhance sensitive signals and extract spectral features for early detection of powdery mildew.

Sub-window Permutation Analysis (SPA) is an effective strategy for variable selection based on Model Population Analysis (MPA)[27]. It has the potential to identify the informative variable with high accuracy and stability. The principle of SPA is to consider the cooperative effects among different variables and to select the informative variables based on the comprehensive analysis of a large number of models with strict statistical criteria. The major contribution of SPA is that, unlike *t* test, it can output a conditional *p* value by implicitly taking into account the synergetic effect of all the other variables. In this sense, the conditional *p* value could help to locate a good combination of informative variables. SPA has been used in discrimination of camellia oil adulteration[28], informative gene selection[29], and revealing informative metabolites[30]. However, it has not been applied and verified in the selection of sensitive variables for crop disease.

In this study, we investigated the feasibility of SPA approach to discriminate the damages of wheat leaves caused by powdery mildew. In the experiment, we chose two varieties of wheat with different disease susceptibility and infected them with *Blumeria graminis*. We systematically tracked the dynamic change patterns of the physiological and biochemical indices (i.e., pigment contents, photosynthetic capacity, and transpiration rate) and used hyperspectral instrument to record spectral responses of wheat leaves at the early infection stage. The sensitive wavebands/indices were extracted by SPA method, and then were used as the inputs for partial least squares linear discriminant analysis (PLS-LDA) method to construct a recognition model. The aims of this study were 1) to illustrate the response characteristics of hyperspectral reflectance within the spectral range of 350 nm - 1000 nm under powdery mildew infection at early stage; 2) to evaluate the performance of features extracted by SPA compared to conventional spectral features; and 3) to develop a PLS-LDA discrimination model to detect wheat powdery mildew at early stage.

2 Materials and methods

2.1 Experimental design

A field experiment was conducted at Pailou experimental station of Nanjing Agricultural University, in Qinhuai District, Nanjing (32°1' N, 118°15' E) from November, 2014 to June, 2015. Two wheat cultivars, Shengxuan 6 (Vh) and Yangfumai 4 (Vm) with high and moderate susceptibility to disease respectively, were used as experimental material. Wheat grown in plots were inoculated with powdery mildew pathogen at the jointing stage (at 137 day after sowing) using prepared pots with infected seedlings, and one row of 6 plots in the east were selected as the disease inducement line, other 6 plots surrounded by plastic film in the upwind direction located in west of the field were chosen as the control with healthy plants, having no inoculation treatment. A randomized complete-block design was used with three replications having a net plot size of 6 m^2 (3 m×2 m). Other practices were conducted according to the local wheat production technology.

2.2 Field measurements

2.2.1 Leaf reflectance measurement

Leaf reflectance was measured with an ASD Field Spec Pro FR2500 spectroradiometer (Analytical Spectral Devices, Boulder, CO, USA)[31]. This instrument records reflectance at 350-1000 nm with a sampling interval of 1.40 nm and a resolution of 3 nm, and at 1000-2500 nm with a sampling interval of 2 nm and a

resolution of 10 nm. The spectrum of white reference panel was recorded once after every 10 minutes. Three readings were recorded from top, middle and bottom parts of each leaf and average of nine readings was calculated to represent leaf reflectance of single leaf. In this study, the bands in the range of 400-1000 nm were retained for further analysis to avoid bands with low signal-to-noise ratio at both ends.

2.2.2 Measurement of leaf chlorophyll contents (LCC)

Right after spectral measurement leaf samples were cut into pieces and 0.1 g of each sample placed in a vial with 25 mL ethanol (95%) for 48 hours for pigment extraction to determine chlorophyll contents. The absorbance of the solution was measured using an UV–Visible spectrophotometer (Hitachi U-2800), at a wavelength of 665, 649 and 470 nm. The chlorophyll a, b and carotenoid concentration were calculated by using the method proposed by Lichtenthaler[32].

2.2.3 Measurement of photosynthetic parameters

Net photosynthesis rate (μmol CO_2 m^{-2} s^{-1}) and transpiration rate (mmol H_2O m^{-2} s^{-1}) were measured at 9:00 to 11:00 am (local time) on clear days, with a portable photosynthesis system LI-6400XT made by (LI-6400, Li-Cor Inc. USA). Same top three leaves used for spectral data of each plant were selected for measurement and three readings per leaf were recorded and average was calculated.

2.2.4 Determination of disease severity (DS)

The diseased leaves were scanned by HP Scanjet G4050 Scanner. Photoshop software 10.0 was used to calculate the lesion area ratio of the entire leaf, which also called lesion ratio (LR). The calculated severity percentage was categorized into nine levels as 0%, 1%, 5%, 10%, 20%, 40%, 60%, 80%, and 100%. For the condition between the grades, the approximate value is taken, as shown in Figure 1. In this article, the disease severity of leaves was qualitatively categorized by two discrete levels: slightly-damaged leaves (those leaves with maximum disease severity of 5%) and healthy leaves.

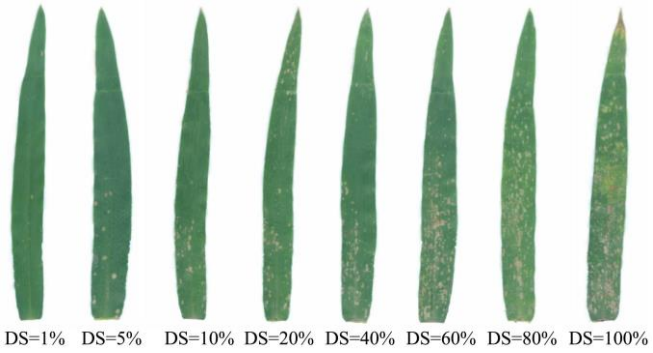

Figure 1 Disease severity (DS) of powdery mildew in wheat leaf

2.3 Methods

2.3.1 Vegetation indices used in this study

In order to assess the suitability of VIs to detect and discriminate among healthy and infected leaves, VIs related to different physiological and biochemical parameters were calculated. In this study 12 vegetation indices and 12 derivative spectral features, most sensitive to these changes were adopted (Table 1).

Table 1 List of vegetation indices and derivative spectral features used in this study

Category	Definition	Formula or description	Reference
Vegetation spectral indices	Narrow-band normalized difference vegetation index, NBNDVI	$(R_{850}-R_{680})/(R_{850}+R_{680})$	[33]
	Triangular vegetation index, TVI	$0.5[120(R750-R550)-200(R670-R550)]$	[34]
	Photochemical reflectance index, PRI	$(R_{531}-R_{570})/(R_{531}+R_{570})$	[35]
	Physiological reflectance index, PhRI	$(R_{550}-R_{531})/(R_{550}+R_{531})$	[35]
	Chlorohpyll absorption ratio index, CARI	$(\lvert a\times 670+R_{670}+b\rvert/(a^2+1)^{0.5})\times(R_{700}/R_{670})$ $a=(R_{700}-R_{500})/150$, $b=R_{550}-(a\times 550)$	[36]
	Transformed chlorophyll absorption ratio index, TCARI	$3\times[(R_{700}-R_{670})-0.2\times(R_{700}-R_{550})\times(R_{700}/R_{670})]$	[37]
	Modified chlorophyll absorption ratio index, MCARI	$[(R701-R671)-0.2\times(R701-R549)]/(R701/R671)$	[38]
	Red-edge vegetation stress index, RVSI	$[(R_{712}+R_{752})/2]-R_{732}$	[39]
	Plant senescence reflectance index, PSRI	$(R_{680}-R_{500})/R_{750}$	[40]
	Anthocyanin reflectance index, ARI	$(R_{550})^{-1}-(R_{700})^{-1}$	[41]
	Structure independent pigment index, SIPI	$(R_{800}-R_{450})/(R_{800}-R_{680})$	[42]
	Normalized pigment chlorophyll ration index, NPCI	$(R_{680}-R_{430})/(R_{680}+R_{430})$	[43]
Derivative spectral features	Maximum value of 1st derivative within blue edge, Db	Blue edge covers 490-530 nm. Db is a maximum value of 1st order derivatives within the blue edge of 35 bands	[44]
	Sum of 1st derivative values within blue edge, SDb	Defined by sum of 1st order derivative values of 35 bands within the blue edge	[44]
	Maximum value of 1st derivative within yellow edge, Dy	Yellow edge covers 550-582 nm. Dy is a maximum value of 1st order derivatives within the yellow edge of 28 bands	[44]
	Sum of 1st derivative values within yellow edge ,SDy	Defined by sum of 1st order derivative values of 28 bands within the yellow edge	[44]
	Maximum value of 1st derivative within red edge ,Dr	Red edge covers 670-737 nm. Dy is a maximum value of 1st order derivatives within the red edge of 61 bands	[44]
	Sum of 1st derivative values within red edge, SDr	Defined by sum of 1st order derivative values of 61 bands within the red edge	[44]
Derivative spectral features	SDr/SDb	The ratio of SDr and SDb	[44]
	SDr/SDy	The ratio of SDr and SDy	[44]
	SDy/SDb	The ratio of SDy and SDb	[44]
	(SDr–SDb)/(SDr+SDb)	The ratio of (SDr–SDb) and (SDr+SDb)	[44]
	(SDy–SDb)/(SDy+SDb)	The ratio of (SDy–SDb) and (SDy+SDb)	[44]
	Wavelength at Dr, REP	REP is wavelength position at Dr	[44]

2.3.2 Features selection by sub-window permutation analysis

Sub-window permutation analysis (SPA) is a new statistical-based distribution and feature selection algorithm in which the cooperative effects of different variables are taken into consideration. The algorithm steps are as follows:

It is called a sub window when SPA extract datasets from both sample size and variable size. This process is repeated N times to obtain N sub training set (X_{train}, Y_{train}) and N sub test set (X_{test}, Y_{test}) with a subset of variables. Then the training set is input to PLS-LDA classifier to get sub models and sub test set is used to predict errors. In all N classifiers, assuming that n ($n \leq N$) classifiers include the variable j, it can be calculated prediction error called Normal Prediction Error (NPE) using the test set k including j ($k \leq n$). When variable j is rearranged, its prediction error can also be obtained which is called Permuted Prediction Error (PPE). This process is repeated in all n tests and provides a set of NPE_k and PPE_k (k = 1, 2,... n).

$$NPE_K = f(X_{test,k}|S_k, H_k),\ k = 1,2,\ldots n \quad (1)$$

$$PPE_K = f(X^r_{test,k}|S_k, H_k),\ k = 1,2,\ldots n \quad (2)$$

where, H_k is the classifier set included j; S_k is the variable set of the classifier k; $X_{test,k}$ is the original k test and $X^r_{test,k}$ is the k test set with variable j rearranged.

Comparing the set of NPE_k and PPE_k:

$$Dmean_j = mean_{j,r} - mean_{j,k} \quad (3)$$

where, $mean_{j,k}$ is the mean value of NPE_k; $mean_{j,r}$ is the mean value of PPE_k.

If $Dmean_j$>0, variable j can improve the prediction ability of the model, which is regarded as a candidate for informative variables, whereas on the contrary, it is called noise variable. For candidate variables, check the distributions of NPE_k and PPE_k through Mann-Whitney U test and calculate the corresponding P value. Then calculate the conditional synergetic score (COSS) to indicate the importance of spectral features and the higher the COSS value is, the more meaningful the variable is. COSS is described as the minus logarithm-transformed P value.

$$COSS = -\mathrm{Log}_{10}(p) \quad (4)$$

2.3.3 Construction of PLS-LDA model for binary classification

Partial least square linear discriminant analysis (PLS-LDA)[45] was employed to classify the healthy and infected leaves. The healthy leaves were without any lesions on the leaf surface denoted by (–1) which were called as negative type. The infected leaves were with lesions just appearing on the leaves and DS was maximum up to 5% (the lesion ratio <7.5%) which were denoted by (+1) and were called as positive type. The performance of the model was evaluated by the variables of confusion matrix as given in table 2. While specificity is the classification accuracy of correctly classified healthy leaves (true negative) and sensitivity or recall is the accuracy of correctly classified infected leaves (true positive). The overall accuracy is given by the mean of specificity and sensitivity which is actually the proportion of all correctly classified healthy and diseased leaves to the total number of leaves.

Table 2 Confusion matrix for binary classification

Category		Predicted	
		Positive	Negative
Actual	Positive	True Positive (TP)	False Negative (FN)
	Negative	False Positive (FP)	True Negative (TN)

Note: evaluation criteria: $Sensitivity = \frac{TP}{TP + FN}$, $Specificity = \frac{TN}{TN + FP}$, $Accuracy = \frac{TP + TN}{TP + FN + FP + TN}$.

2.3.4 Calibration and validation

In this study, the data of Vm were used as calibration data set. The sample sizes were 168, 77 infected leaves and 91 healthy leaves. The data of Vh were used as validation data set. The leaf sample size were 167, among which there were 81 infected leaves and 86 healthy leaves. The detailed data is shown in Table 1. All the calculations are conducted with self-programming software under MATLAB R2015b.

Table 3 The calibrated and validated data with varying proportions of lesions

Cultivar	Proportions of lesions				Total	Positive	Negative	Function
	0%	0-1%	1-2.5%	2.5-7.5%				
Vm	91	40	27	10	168	77	91	Calibration
Vh	86	29	22	30	167	81	86	Validation

3 Results

3.1 Changes of leaf reflectance with different disease severity

The dynamic change curves of DS of wheat leaves with high sensitivity to powdery mildew are shown in Figure 2a. After inoculation, the lower leaf (T4) was infected first. With the aggravation of DS, the lesions started appearing on the top third (T3) and the top second (T2) leaves at 7-10 days after inoculation (DAI). At 20-25 DAI (at heading stage), the lesions started appearing on the top first (T1) leaf. At 28-30 DAI (at flowering and grain filling stage), the disease outbreak was maximum.

Analyses of the changes in spectral reflectance and its sensitivity to different disease severity levels indicated that the differences in reflectance of wheat leaves were smaller at the early stage but with the aggravation of DS , the spectral reflectance in the visible range (400-700 nm) and the near infrared waveband (760-1000 nm) displayed an increasing trend (Figure 2b). This phenomenon was more obvious in the absorption valley of 680 nm.

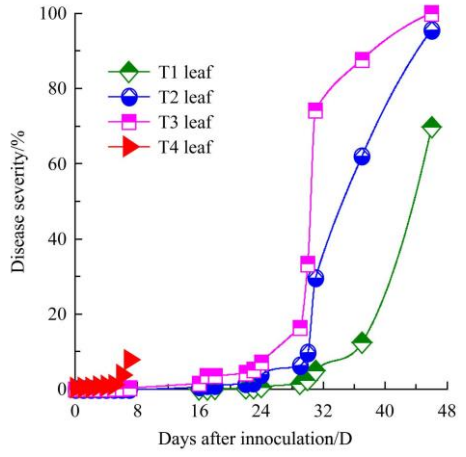

a.

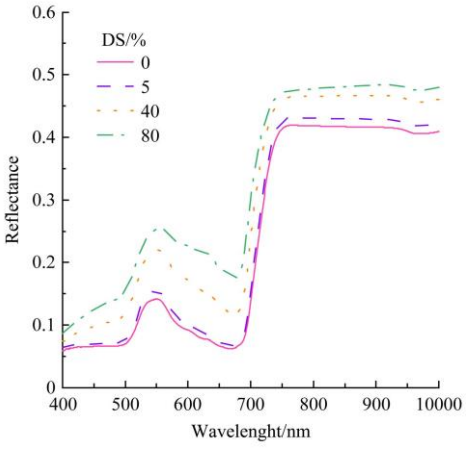

b.

Figure 2 Dynamic changes of disease severity of leaves (DS) with the days after inoculation (DAI) (a) and the changes in the spectral reflectance of wheat Vh leaves with DS (b)

3.2 Dynamic Change patterns of Pigment Contents and Photosynthetic Capacity

Dynamic change patterns of chlorophyll (Chl) contents and carotenoids (Car) contents of T1, T2 and T3 leaves of Vh after being infected *by Blumeria graminis* are shown in Figure 3. At the early stage of infection, there are no significant differences in Chl and Car contents of the normal and infected leaves. As the days passed after inoculation, both Chl and Car contents were significantly reduced and exhibited the same trends in both cultivars. The changes in Car contents were relatively slower as compared to Chl contents.

Moreover, investigation of the dynamic change patterns of net photosynthetic rate (Pn) and transpiration rate (Tr) of T1, T2 and T3 leaves after inoculation demonstrated slight increasing trends at early stage but the values of both parameters decreased significantly with the increasing disease severity. These changes were consistent with those of pigment contents. In terms of different leaf positions, Pn and Tr of T1 and T2 leaves were significantly reduced with the aggravation of DS, but the differences in these parameters of T3 leaf were relatively smaller.

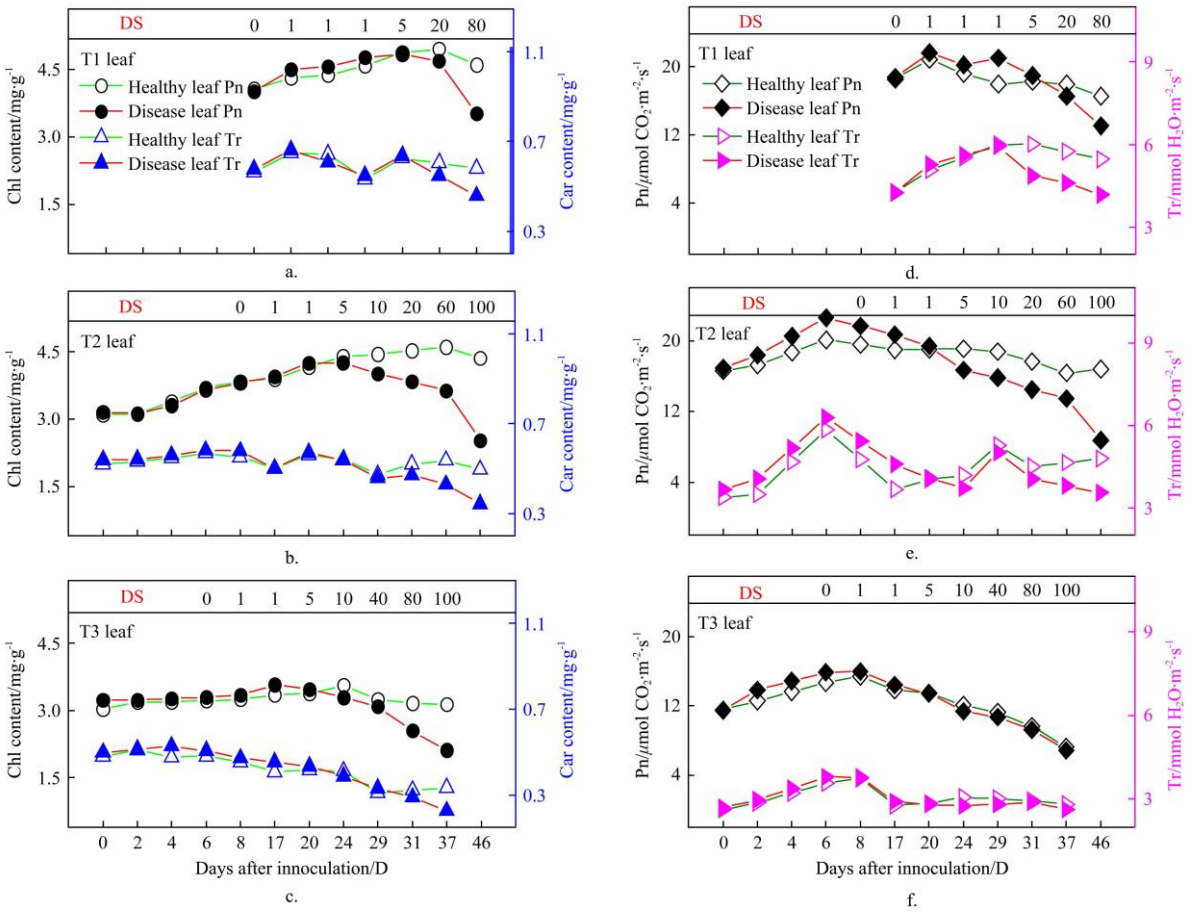

Figure 3 The dynamic changes of LCC and Car contents (a, b, c) and Pn and Tr (d, e, f) of Vh with days after inoculation (DAI)

3.3 Spectral feature extraction

Spectral features for recognition of wheat powdery mildew at early stage were extracted with SPA method from spectral reflectance with the wavebands ranging from 400-1000 nm and from 24 indices calculated in this study, which were written as SPA + wavelength and SPA + spectral index. It was compared to the features with that of sensitive wavebands and spectral indices selected with correlation analysis as shown in Figure 4 and Figure 5, respectively. The sensitive wavebands and sensitive indices were selected based on the relationship between the spectral wavebands and spectral indices with DS at $p<0.01$. The leaf spectrum of the varieties Vh and Vm were significantly correlated with the severity of the disease at early stage at 675-700 nm and 711-1000 nm at $p<0.01$ (Figure 4). Thus, these two ranges of 316 bands can be used as spectral features for the identification of wheat leaf health and total 24 spectral indices are significantly correlated to disease severity at $p<0.01$ (Figure 5).

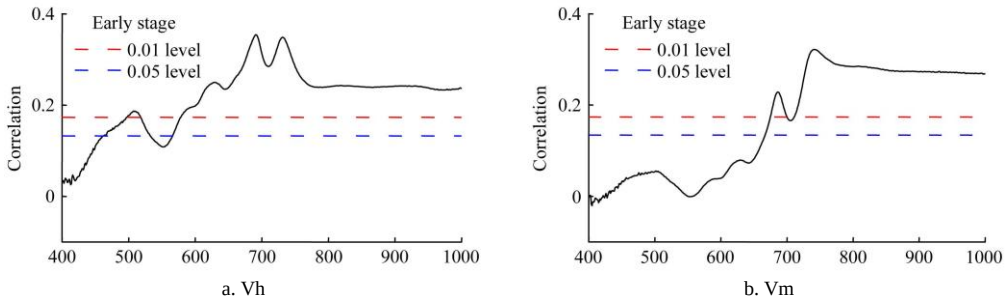

a. Vh b. Vm

Figure 4 Coefficient of correlation (r) for the linear correlation between the spectral reflectance of wheat leaves and disease severity for (a) variety Vh and (b) variety Vm

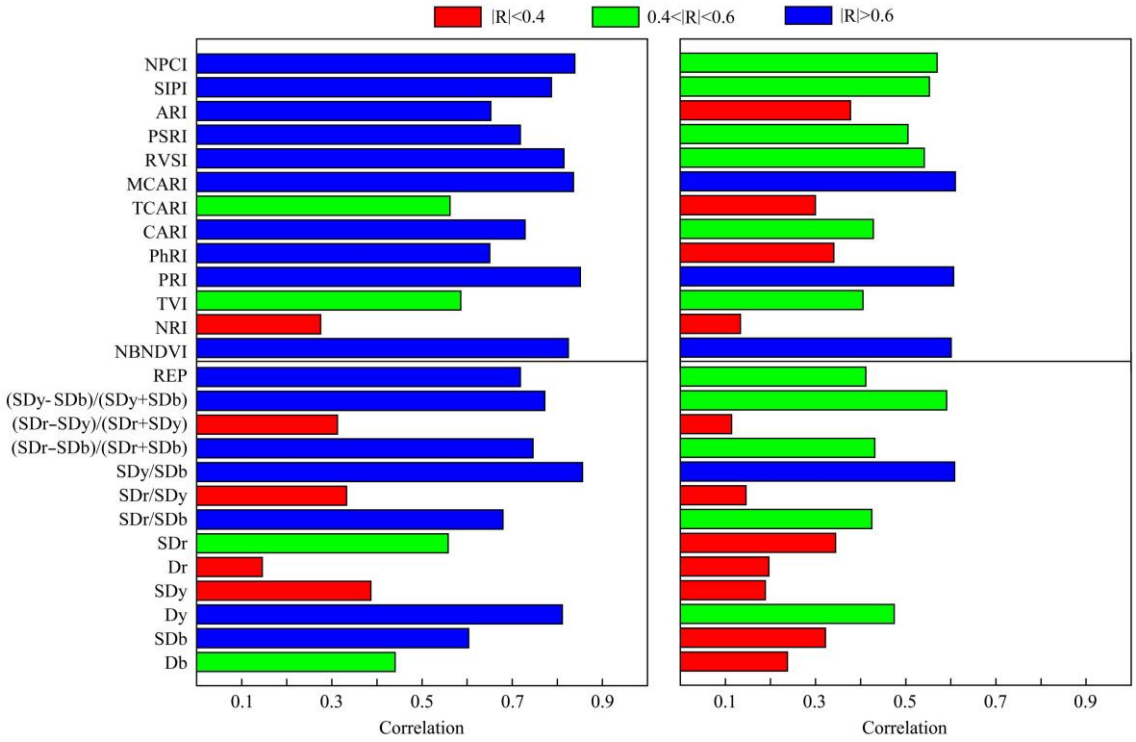

a. Vh b. Vm

Figure 5 Coefficient of correlation (r) for the linear correlation between the spectral indices and disease severity for (a) variety Vh and (b) variety Vm

3.3.1 Sensitive wavelength extracted by using SPA

By using SPA algorithm, we calculated the statistical distributions before and after the position rearrangement of each wavelength within the range of 400-1000 nm, and ranked the order of the importance of each wavelength based on COSS values (Figure 6a). The COSS values which were ranked the first 20 places were 554, 569, 550, 739, 747, 749, 755, 814, 631, 757, 433, 428, 732, 740, 746, 786, 761, 596, 750 and 768 nm. Among these, number of wavebands in the red edge region were highest. This is related to the highest coefficient for the correlation of spectral features in the red edge region with DS.

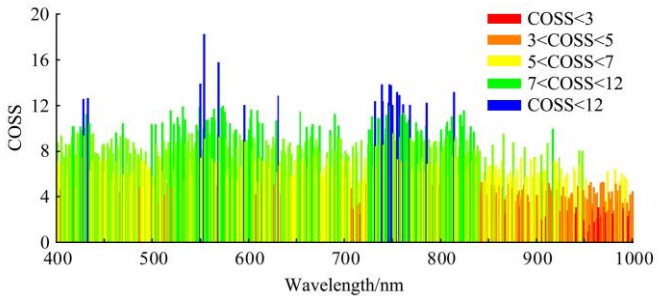

a.

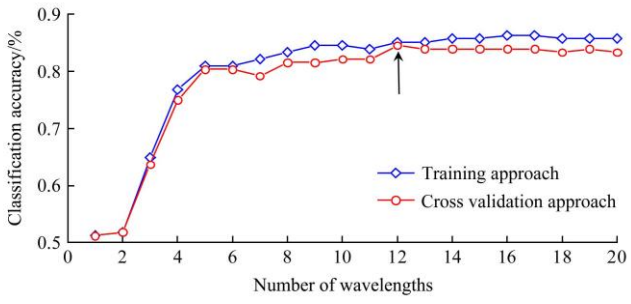

b.

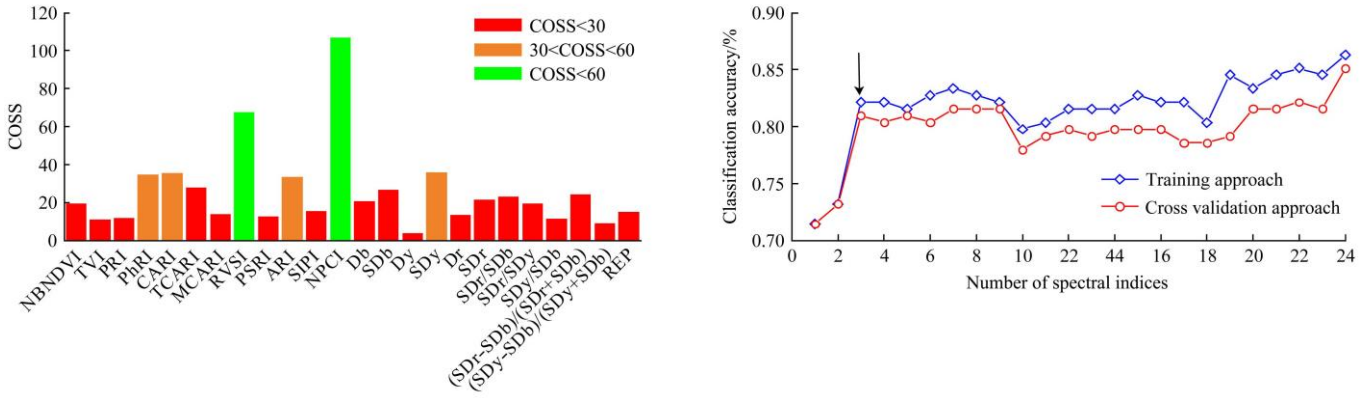

c. d.

Figure 6 COSS values of each feature wavelength (a) and each spectral index calculated by SPA algorithm (c) and the changes in PLS-LDA accuracy generated by full data training and cross-validation in feature bands (b) and spectral indices (d) with different numbers of wavebands

We can see that in calibration mode (Figure 6b), the overall accuracy curve was monotonous, after the number reached 5, the overall accuracy was maintained in a certain range with fluctuations of small extent and reached the maximal value when the number of wavebands reached 16.

In the validation mode, the accuracy was highest when the number of wavebands reached 12, thus, the first 12 wavebands were selected as the preliminary feature set extracted by SPA.

3.3.2 Sensitive spectral indices extracted by SPA

By using the same method described above the optimal combination of spectral indices was extracted from the available spectral indices to establish the recognition model for the health status of wheat leaves. Results indicated that the first ten spectral indices were NPCI RVSI, SDy, CARI, PhRI, ARI, TCARI, SDb, (SDr–SDb)/(SDr+SDb) and SDr/SDb (Figure 6c.).

Similarly, in both modes, the overall accuracy of the PLS-LDA model for the health status of wheat leaves constructed with different numbers of spectral indices was evaluated (Figure 6d.). The first 3 spectral indices i.e. were NPCI, RVSI and SDY with the highest COSS values were selected for diagnosis of the health status of wheat leaves.

3.4 Calibration and validation of the recognition model

The extracted spectral features mentioned above were used as the input variables in PLS-LDA recognition model for classification of healthy and diseased leaves. Calibration and Leave-One-Out Cross validation (LOOCV) of model was performed with the data of variety (Vm) and independent variety validation (IVV) was performed with the data of variety (Vh).

Table 4 and 5 show that in terms of wavelength, when the sensitive wavebands (316) were used to judge the health status of wheat leaves, the classification accuracies in calibration could reach over 90%. But the performance of the validation in IVV was quite poor with the overall accuracy of only 65.27%, which indicates that the sensitive wavebands conventionally selected by correlation analysis are not suitable and stable for the diagnosis of the health status of wheat leaves of different cultivars and data, and also increase computational cost by using as many as 316 variables. While the model constructed with SPA + wavelength features was more stable by utilizing only 12 sensitive variables with the overall calibration, LOOCV and IVV validation accuracies of 85.12, 84.52 and 84.43% respectively. The calibration, LOOCV and IVV classification accuracies of PLS-LDA model based on 3 features extracted by SPA + spectral indices were 82.14, 80.95 and 85.63% respectively. Though the calibration accuracy of model based on SPA + spectral indices was a bit less than that based on 24 sensitive spectral indices but its overall classification performance was best with less number of features, low computational cost and stable LOOCV and IVV validation results. The results also showed that the sensitivity of the classification model was always greater than specificity.

Table 4 Calibration of recognition model

Spectral features		Feature number	Model of calibration			
			Spec.	Sens.	Accu./%	AUC/%
Wavelength	Sensitive wavelength	316	98.68	97.83	98.21	98.26
	SPA + wavelength	12	83.33	86.67	85.12	85.00
Spectral index	Sensitive spectral index	24	80.49	87.21	83.93	83.85
	SPA + spectral index	**3**	78.31	85.88	82.14	82.10

Note: Sensitivity: Sens; Specificity: Spec; Accuracy (%) : Accu; AUC: area under the curve (%).

Table 5 Validation of recognition model

Spectral features		Feature number	Model of validation							
			LOOCV				IVV			
			Spec.	Sens.	Accu./%	AUC/%	Spec.	Sens.	Accu/%	AUC/%
Wavelength	Sensitive wavelength	316	92.31	94.44	93.38	93.45	60.75	73.33	65.27	67.04
	SPA + wavelength	12	83.12	85.71	84.52	84.42	83.13	85.71	84.43	84.42

Spectral index	Sensitive spectral index	24	75.00	83.33	79.17	79.17	78.31	80.95	79.64	79.63
	SPA + Spectral index	3	77.78	83.91	80.95	80.84	86.08	85.23	85.63	85.65

4 Discussion

4.1 Changes in Leaf Physiological Parameters

Pigments are the important parameters indicating the growth and nutritional status and biotic and abiotic stresses of crops[40,46]. Thus, clear understanding of the dynamic responses of crop pigments to biotic and abiotic stresses is important and helpful for rapid diagnosis of crop diseases. The results revealed that the leaf pigment responded slowly to the powdery mildew with a slight increasing trend first at the early infection stage (Figure 3a, b & c), probably due to the natural resistance response of plants when confronting any stress. With the increase of DS, the pigment contents of leaves reduced rapidly (Figure 3a, b & c) that is consistent with previous studies of Feng et al.[8], Cao et al.[47], and Wang et al.[48]. The increase of DS also caused the stomatal structure of leaves to deteriorate, further leading to continuous reduction of leaf water contents[49-51] and accelerated Chlorophyll degradation. Moreover, we found that the LCC of Vh reduced more rapidly as compared to that of Vm after the inoculation. It is suggested that different wheat varieties respond differently to powdery mildew.

Monitoring the changes in the photosynthetic capacity of crops under disease stress is important to understand the variations in the internal physiological mechanisms of plants in response to disease. It is noticed that with the appearance of disease symptoms, the changes in photosynthesis and transpiration rates were smaller with slightly increasing values at the early stage of disease and then decreased as the DS increased, similar to that of chlorophyll contents (Figure 3d, e, & f). A slight increasing response at early stage is may be due to the self-mechanism of plants to resist external stresses and to maintain the normal physiological activities[52]. Photosynthetic capacity of plants is affected by many factors such as physical, chemical, thermal, nutrients, water and disease stresses. We found that with the increase of disease severity and lesion ratio on the leaves, the leaf epidermis and tissues structures are destroyed (Figure 1). Therefore, the chloroplast of leaves is destroyed which led to reduction of chlorophyll contents and photosynthetic rate of plants. Additionally, stomatal closure and reduction of leaf moisture contents in response of disease, could also cause reduction of photosynthetic and transpiration rate. Moreover, Pn and Tr rate of T3 leaves (Figure 3f) were relatively smaller than T1 and T2 which indicated that *Blumaria graminis* caused more significant effects on the photosynthetic capacity of major functional leaves.

Disease development was slow initially, but it became more serious and increased dramatically by the flowering stage (Figure 2a). Thus, it can be proposed that the first 20 days after infection are important and a key period for diagnosis, prevention and possible control of wheat powdery mildew.

4.2 Leaf spectral reflectance

The pigment, nitrogen, water and other nutritional substances in the leaves decrease when the crop is under disease stress, and the spectral reflectance in the visible light range is increased[10,35]. This change has been observed in different types of crops affected with different plant diseases[20,53,54]. Our study also showed similar results with significant increase in spectral reflectance at visible region and a slight and non-significant increase at near infrared range under powdery mildew stress (Figure 2b). Some studies found that the spectral reflectance in near infrared band was reduced at both leaf scale[15] and canopy scale[55,56]. At canopy scale, the spectral reflectance features are more affected by leaf area, water, and soil background. When crop is under disease stress, the leaf area index of the canopy layer and the water contents are reduced, leading to the reduction in spectral reflectance in near infrared bands. However, at leaf scale, due to the disposition and accumulation of the white moldy layer on the leaf surface could affect the reflectance to increase in both visible and NIR region, which might balance the effects from breakdown of leaf cell structures, and making the reflectance to increase in the NIR region but the increase was insignificant.

Under disease stress, the sensitivities to disease in the visible band were higher than that in the near infrared band[57-59]. It is indicated that with the aggravation of DS, the damage caused by powdery mildew is larger to leaf pigments than that to the intracellular structure. However, at early stage, the leaf spectral response to the disease was relatively low (Figure 2b). The coefficient of the maximal correlation in the red infrared band was also lower than 0.4 (Figure 4). This is because at the early stage of disease, the pathogenic fungi mainly multiplied, but the damage caused by fungus was not obvious. At this stage, no obvious changes in biochemical components of plants were observed, the same effect has also been reported by Bushnell et al.[60]. With the aggravation of DS, visible symptoms started appearing on leaves and thus caused a series of spectral feature responses. In addition, the powdery mildew symptoms at initial stage of infection mainly distributed on the leaf edges. However, the central parts of the leaves were measured by spectral instruments during the experimental processes. The reasons for appearance of the lesions on the leaf edges at the early stage of disease are unclear.

4.3 SPA method for disease feature extraction

The hyper-spectral data have the problems of large noise,

multi-collinearity and complicated redundancy. To achieve the diagnosis and recognition of the health status of leaves, it is extremely important to select the appropriate methods for extraction of spectral features. SPA is a new statistics-based distribution feature selection algorithm, considering the cooperative effect among different variables. The advantage of SPA algorithm is the combination of the model-based cluster analysis and rearrangement-based method of Random forest. The screening of the informative variables is not based on the single model, but based on a comprehensive analysis of a large number of models and the use of the strict statistical tests. The informative variables obtained by SPA are statistically significant and stable. The calibration and validation accuracies of classification model based on features extracted by SPA method were higher and stable with less number of variables, as compared to that of selected by empirical and conventional method (Table 4 and 5). Therefore, SPA has the potential to diagnosis and recognition of the health status of leaves.

Sun et al.[28] conducted discriminating recognition of the complicated adulteration of camellia oil with near infrared spectral feature extracted by using SPA. The results indicated that SPA method could effectively screen out the feature wavelengths, simplified model and improved the prediction accuracy and stability of the model. Currently, SPA method has not been applied in agricultural remote sensing field. Our results could provide a reference for the introduction of SPA method in the field of agricultural remote sensing.

5 Conclusions

In this study, our results demonstrated that the SPA coupled with PLS-LDA method based on sensitive bands and VIs has been successfully employed to identify wheat leaves infected with *Blumaria graminis* at early stage. On the basis of conventionally selected sensitive bands based on correlation analysis, the calibration classification accuracy of PLS-LDA model reached 98.21%, but this model did not pass the independent variety validation test (IVV) showing an accuracy of only 65.27%, indicating that the model has high computational cost of 316 variables and is not suitable and stable for diagnosis of the health status of wheat leaves of different cultivars. While the number of feature bands extracted with SPA technique were only 12. The calibration, LOOCV and independent variety validation (IVV) classification accuracies of the model were 85.12, 84.52 and 84.43% respectively. Similarly, calibration, LOOCV and independent variety validation (IVV) accuracies of PLS-LDA model established by3 spectral indices extracted with SPA based technique were 82.14, 80.95 and 85.63% respectively. Our results indicated that the sensitive wavebands selected with SPA technique are of statistical significance and the established model is highly stable. Therefore, such a method can be an efficient and economical substitute to conventional methods, especially in case of high throughput hyperspectral information. On the basis of these results certain sensors for practical use to detect plant diseases at early stage in crop fields can be developed in future. The applicability of this method can be tested and verified for other plant pathogen systems for the early and pre-symptomatic detection of biotic stresses in future.

Acknowledgments

This work was supported by grants from the National Key Research and Development Plan of China (2016YFD0200700), National Natural Science Foundation of China (31671582), Jiangsu Qinglan Project, the Jiangsu Collaborative Innovation Center for Modern Crop Production (JCICMCP), Jiangsu Province Key Technologies R&D Program (BE2016375), the Academic Program Development of Jiangsu Higher Education Institutions (PAPD), and the 111 project (B16026). Finally, we would like to thank the reviewers for recommendations which improved the manuscript.

[References]

[1] Huang L, Ding W, Liu W, Zhao J, Huang W, Xu C, Zhang D, Liang D. Identification of wheat powdery mildew using in-situ hyperspectral data and linear regression and support vector machines. Journal of Plant Pathology, 2019; 101(4): 1–11. doi: 10.1007/s42161-019-00334-2.

[2] Mohd Asaari M S, Mishra P, Mertens S, Dhondt S, Inzé D, Wuyts N, Scheunders P. Close-range hyperspectral image analysis for the early detection of stress responses in individual plants in a high-throughput phenotyping platform. ISPRS journal of photogrammetry and remote sensing, 2018; 138: 121–138. doi: 10.1016/j.isprsjprs.2018.02.003.

[3] Christ B J, Petersen G, Ressler L, Warmer E. Early detection of potato late blight using hyperspectral remote sensing, 2000.

[4] Rumpf T, Mahlein A K, Steiner U, Oerke E C, Dehne H W, Plümer L. Early detection and classification of plant diseases with support vector machines based on hyperspectral reflectance. Computers and electronics in agriculture, 2010; 74(1): 91–99. doi: 10.1016/j.compag.2010.06.009.

[5] Lorenzen B, Jensen A. Changes in leaf spectral properties induced in barley by cereal powdery mildew. Remote Sensing of Environment, 1989; 27(2): 201–209. doi: 10.1016/0034-4257(89)90018-7.

[6] Graeff S, Link J, Claupein W. Identification of powdery mildew (Erysiphe graminis sp. tritici) and take-all disease (Gaeumannomyces graminis sp. tritici) in wheat (*Triticum aestivum* L.) by means of leaf reflectance measurements. Central European Journal of Biology, 2006; 1(2): 275–288. doi: 10.2478/s11535-006-0020-8.

[7] Baret F, Vanderbilt V C, Steven M D, Jacquemoud S. Use of spectral analogy to evaluate canopy reflectance sensitivity to leaf optical properties. Remote Sensing of Environment, 1994; 48(2): 253–260. doi: 10.1016/0034-4257(94)90146-5.

[8] Feng W, Wang X Y, Song X, He L, Wang C, Guo T. Hyperspectral estimation of canopy chlorophyll density in winter wheat under stress of powdery mildew. Transactions of the Chinese Society of Agricultural Engineering, 2013; 29(13): 114–123. doi: 10.3969/j.issn.1002-6819.2013.13.016.

[9] Miller J R, Wu J, Boyer M G, Belanger M, Hare E W. Seasonal patterns in leaf reflectance red-edge characteristics. International Journal of Remote Sensing, 1991; 12(7): 1509–1523. doi: 10.1080/01431169108955186.

[10] Devadas R, Lamb D W, Simpfendorfer S, Backhouse D. Evaluating ten spectral vegetation indices for identifying rust infection in individual wheat leaves. Precision Agriculture, 2009; 10(6): 459–470. doi: 10.1007/s11119-008-9100-2.

[11] Huang W, Lamb D W, Niu Z, Zhang Y , Liu L , Wang J . Identification of yellow rust in wheat using in-situ spectral reflectance measurements and airborne hyperspectral imaging. Precision Agriculture, 2007; 8(4): 187–197. doi: 10.1007/s11119-007-9038-9.

[12] Huang W, Guan Q, Luo J, Zhang J, Zhao J, Liang D, Huang L, Zhang D. New optimized spectral indices for identifying and monitoring winter wheat diseases. IEEE Journal of Selected Topics in Applied Earth Observations and Remote Sensing, 2014; 7(6): 2516–2524. doi: 10.1109/JSTARS.2013.2294961.

[13] Mahlein A K, Rumpf T, Welke P, Dehne H W, Plümer L, Steiner U, Oerke E C. Development of spectral indices for detecting and identifying plant diseases. Remote Sensing of Environment, 2013; 128: 21–30. doi: 10.1016/j.rse.2012.09.019.

[14] Zheng Q, Huang W, Cui X, Dong Y, Shi Y, Ma H, Liu L. Identification of wheat yellow rust using optimal three-band spectral indices in different growth stages. Sensors, 2019; 19(1): 35. doi: 10.3390/s19010035.

[15] Zhang J C, Pu R L, Wang J H, Huang W J, Yuan L, Luo J H. Detecting powdery mildew of winter wheat using leaf level hyperspectral

measurements. Computers and Electronics in Agriculture, 2012; 85: 13–23. doi: 10.1016/j.compag.2012.03.006.

[16] Cao X, Luo Y, Zhou Y, Duan X, Cheng D. Detection of powdery mildew in two winter wheat cultivars using canopy hyperspectral reflectance. Crop Protection, 2013; 45: 124–131. doi: 10.1016/j.cropro.2012.12.002.

[17] Sankaran S, Mishra A, Ehsani R, Davis C. A review of advanced techniques for detecting plant diseases. Computers and Electronics in Agriculture, 2010; 72(1): 1–13. doi: 10.1016/j.compag.2010.02.007.

[18] Liu Z Y, Huang J F, Shi J J, Tao R X, Zhou W, Zhang L L. Characterizing and estimating rice brown spot disease severity using stepwise regression principal component regression and partial least-square regression. Journal of Zhejiang University Science B, 2007; 8(10): 44–50. doi: 10.1631/jzus.2007.B0738.

[19] Liu Z Y, Qi J G, Wang N N, Zhu Z R, Luo J, Liu L J, Tang J, Cheng J A. Hyperspectral discrimination of foliar biotic damages in rice using principal component analysis and probabilistic neural network. Precision Agriculture, 2018; 19: 973–991. doi: 10.1007/s11119-018-9567-4.

[20] Cheng T, Rivard B, Sánchez-Azofeifa G A, Feng J, Calvo-Polanco M. Continuous wavelet analysis for the detection of green attack damage due to mountain pine beetle infestation. Remote Sensing of Environment, 2010; 114(4): 899–910. doi: 10.1016/j.rse.2009.12.005.

[21] Shi Y, Huang W, González-Moreno P, Luke B, Dong Y, Zheng Q, Ma H, Liu L. Wavelet-based rust spectral feature set (WRSFs): a novel spectral feature set based on continuous wavelet transformation for tracking progressive host–pathogen interaction of yellow rust on wheat. Remote Sensing, 2018; 10(4): 525. doi: 10.3390/rs10040525.

[22] Muhammed H H. Hyperspectral crop reflectance data for characterising and estimating fungal disease severity in wheat. Biosystems Engineering, 2005; 91(1): 9–20. doi: 10.1016/j.biosystemseng.2005.02.007.

[23] Muhammed H H, Larsolle A. Feature vector based analysis of hyperspectral crop reflectance data for discrimination and quantification of fungal disease severity in wheat. Biosystems engineering, 2003; 86(2): 125–134. doi: 10.1016/S1537-5110(03)00090-4.

[24] Moshou D, Bravo C, West J, Wahlen S, McCartney A, Ramon H. Automatic detection of 'yellow rust'in wheat using reflectance measurements and neural networks. Computers and electronics in agriculture, 2004; 44(3): 173–188. doi: 10.1016/j.compag.2004.04.003.

[25] Moshou D, Bravo C, Oberti R, West J, Bodria L, McCartney A, Ramon H. Plant disease detection based on data fusion of hyper-spectral and multi-spectral fluorescence imaging using Kohonen maps. Real-Time Imaging, 2005; 11(2): 75–83. doi: 10.1016/j.rti.2005.03.003.

[26] Yuan L, Zhang J, Zhao J, Huang L, Yang X, Wang J. Mapping of powdery mildew using multi-spectral HJ-CCD image in Beijing suburban area. Optik-International Journal for Light and Electron Optics, 2013; 124(21): 4734–4738. doi: 10.1016/j.ijleo.2013.01.103.

[27] Li H D, Liang Y Z, Xu Q S, Cao D S. Model population analysis for variable selection. Journal of Chemometrics, 2010; 24(7-8): 418–423. doi: 10.1002/cem.1300.

[28] Sun T, Wu Y, Li X. Discrimination of camellia oil adulteration by NIR spectra and subwindow permutation analysis. Acta Optica Sinica, 2015; 35(6): 350–370. doi: 10.3788/AOS201535.0630005. (in Chinese).

[29] Wang Q, Li H D, Xu Q S, Liang Y Z. Noise incorporated subwindow permutation analysis for informative gene selection using support vector machines. The Analyst, 2011; 136(7): 1456–1463. doi: 10.1039/c0an00667j.

[30] Li H D, Zeng M M, Tan B B, Liang Y Z, Xu Q S, Cao D S. Recipe for revealing informative metabolites based on model population analysis. Metabolomics, 2010; 6(3): 353–361. doi: 10.1007/s11306-010-0213-z.

[31] Hatchell D C. ASD Technical guide. Analytical Spectral Devices Inc, 1999; 5335.

[32] Lichtenthaler H K. Chlorophylls and carotenoids: pigments of photosynthetic biomembranes. Methods in enzymology, 1987; 148: 350–382. doi: 10.1016/0076-6879(87)48036-1.

[33] Thenkabail P S, Smith R B, Pauw E D. Hyperspectral vegetation indices and their relationships with agricultural crop characteristics. Remote sensing of Environment, 2000; 71(2): 158–182. doi: 10.1016/s0034-4257(99)00067-x.

[34] Broge N H, Leblanc E. Comparing prediction power and stability of broadband and hyperspectral vegetation indices for estimation of green leaf area index and canopy chlorophyll density. Remote sensing of environment, 2001; 76(2): 156–172. doi: 10.1016/s0034-4257(00)00197-8.

[35] Gamon J A, Penuelas J, Field C B. A narrow-waveband spectral index that tracks diurnal changes in photosynthetic efficiency. Remote Sensing of environment, 1992; 41(1): 35–44. doi: 10.1016/0034-4257(92)90059-s.

[36] Kim M S, Daughtry C S T, Chappelle E W, McMurtrey J E, Walthall C L. The use of high spectral resolution bands for estimating absorbed photosynthetically active radiation (A par), 1994.

[37] Haboudane D, Miller J R, Tremblay N, Zarco-Tejada P J, Dextraze L. Integrated narrow-band vegetation indices for prediction of crop chlorophyll content for application to precision agriculture. Remote sensing of environment, 2002; 81(2-3): 416–426. doi: 10.1016/s0034-4257(02)00018-4.

[38] Daughtry C S T, Walthall C L, Kim M S, De Colstoun E B, McMurtrey Iii J E. Estimating corn leaf chlorophyll concentration from leaf and canopy reflectance. Remote sensing of Environment, 2000; 74(2): 229–239. doi: 10.1016/S0034-4257(00)00113-9.

[39] Merton R, Huntington J. Early simulation results of the ARIES-1 satellite sensor for multi-temporal vegetation research derived from AVIRIS, 1999; 9–11.

[40] Merzlyak M N, Gitelson A A, Chivkunova O B, Rakitin V Y U. Non-destructive optical detection of pigment changes during leaf senescence and fruit ripening. Physiologia plantarum, 1999; 106(1): 135–141. doi: 10.1034/j.1399-3054.1999.106119.x.

[41] Gitelson A A, Merzlyak M N, Chivkunova O B. Optical properties and nondestructive estimation of anthocyanin content in plant leaves. Photochemistry and photobiology, 2001; 74(1): 38–45. doi: 10.1562/0031-8655(2001)074<0038:opaneo>2.0.co;2.

[42] Penuelas J, Baret F, Filella I. Semi-empirical indices to assess carotenoids/chlorophyll a ratio from leaf spectral reflectance. Photosynthetica, 1995; 31(2): 221–230.

[43] Peñuelas J, Gamon J A, Fredeen A L, Merino J, Field C B. Reflectance indices associated with physiological changes in nitrogen-and water-limited sunflower leaves. Remote sensing of Environment, 1994; 48(2): 135–146. doi: 10.1016/0034-4257(94)90136-8.

[44] Gong P, Pu R, Heald R C. Analysis of in situ hyperspectral data for nutrient estimation of giant sequoia. International Journal of Remote Sensing, 2002; 23(9): 1827–1850. doi: 10.1080/01431160110075622.

[45] Barker M, Rayens W. Partial least squares for discrimination. Journal of Chemometrics: A Journal of the Chemometrics, 2003; 17(3): 166–173. doi: 10.1002/cem.785.

[46] Peñuelas J, Filella I. Visible and near-infrared reflectance techniques for diagnosing plant physiological status. Trends in plant science, 1998; 3(4): 151–156. doi: 10.1016/S1360-1385(98)01213-8.

[47] Cao X, Zhou Y, Duan X, Cheng D. Relationships between canopy reflectance and chlorophyll contents of wheat infected with powdery mildew in fields. Acta Phytopathologica Sinica, 2009; 39(3): 290–296. doi: CNKI:SUN:ZWBL.0.2009-03-010. (in Chinese)

[48] Wang X, Feng W, Yang Y, Hou C, Wang C, Guo T. Relationship of physiological indices and yield loss of wheat with severity level of powdery mildew. Journal of Triticeae Crops, 2012; 32(6): 1192–1198. doi: 10.7606/j.issn.1009-1041.2012.06.032. (in Chinese)

[49] Li Y R, Shang H S. Changes in water relations of wheat leaves in the infection process of stripe rust. Acta Phytopathologica Sinica, 2000; 26(6): 471–475. doi: 10.3321/j.issn:1671-3877.2000.06.002. (in Chinese)

[50] Wang B H, Huang M Y, Ma Z H, Wang J H. Effects of stripe rust on chlorophyll fluorescence and photosynthesis of winter wheat. Acta Agriculturae Boreali—Sinica, 2004; 19(2): 92–94. doi: 10.3321/j.issn:1000-7091.2004.02.023. (in Chinese)

[51] Duniway J M, Durbin R D. Some effects of Uromyces phaseoli on the transpiration rate and stomatal response of bean leaves. Phytopathology, 1971; 61(1): 114–119. doi: 10.1094/Phyto-61-114.

[52] Smith R C G, Heritage A D, Stapper M, Barrs H.D. Effect of stripe rust (Puccinia striiformis West.) and irrigation on the yield and foliage temperature of wheat. Field Crops Research, 1986; 14(1): 39–51. doi: 10.1016/0378-4290(86)90045-6.

[53] Huang M Y, Wang J H, Huang W J, Huang Y D, Zhao C J, Wan A M. Hyperspectral character of stripe rust on winter wheat and monitoring by remote sensing. Transactions of the CSAE, 2003; 19(6) 154–158. doi: 10.3321/j.issn:1002-6819.2003.06.037. (in Chinese)

[54] Chen B, Wang K, Li S, Jin X, Chen J, Zhang D. The effects of disease stress on spectra reflectance and chlorophyll fluorescence characteristics of cotton leaves. Transactions of the CSAE, 2011; 27(9): 86–93. doi: 10.3969/j.issn.1002-6819.2011.09.017. (in Chinese)

[55] Liu L, Song X, Li C, Qi L, Huang W, Wang J. Monitoring and evaluation

of the diseases of and yield winter wheat from multi-temporal remotely-sensed data. Transactions of the CSAE, 2009; 25(1): 137–143. doi: CNKI:SUN:NYGU.0.2009-01-033. (in Chinese)

[56] [56] Guo J B, Huang C, Wang H G, Sun Z Y, Ma Z H. Disease index inversion of wheat stripe rust on different wheat varieties with hyperspectral remote sensing. Spectroscopy and Spectral Analysis, 2009; 29(12): 3353–3357. doi: 10.3964/j.issn.1000-0593(2009)12-3353-05. (in Chinese)

[57] Zhang D Y, Zhang J C, Huang W J. Investigation of the hyperspectral image characteristics of wheat leaves under different stress. Spectroscopy and Spectral Analysis, 2011; 31(4): 1101–1105. doi: 10.3964/ j.issn.1000-0593(2011)04-1101-05. (in Chinese)

[58] Jing X, Huang W J. Hyperspectral inversion models on verticillium wilt severity of cotton leaf. Spectroscopy and Spectral Analysis, 2009; 29(12): 3348–3352. doi: 10.3964/j.issn.1000-0593(2009)12-3348-05. (in Chinese)

[59] Cheng S X, Shao Y N, Wu D, He Y. Determination of rice leaf blast disease level based on visible near infrared spectroscopy. Journal of Zhejiang University (Agriculture and Life Sciences), 2011; 37(3): 307–311. doi: 10.3785/j.issn.1008-9209 .2011 .03.011. (in Chinese)

[60] Bushnell W R. Structural and physiological alterations in susceptible host tissue. The cereal rusts, 1984; 1: 477–507. doi: 10.1016/ B978-0-12-148401-9.50021-2.